

Dissociation of N_2 in capture and ionization collisions with fast H^+ and N^+ ions and modeling of positive ion formation in the Titan atmosphere

H. Luna,¹ M. Michael,² M. B. Shah,¹ R. E. Johnson,² C. J. Latimer,¹ and J. W. McConkey³

Received 17 June 2002; revised 14 August 2002; accepted 19 November 2002; published 30 April 2003.

[1] Electron capture and ionization cross sections for protons and nitrogen ions incident on N_2 are measured in the energy range 10–100 keV using time of flight (TOF) coincidence counting techniques. In the case of proton impact the formation of N_2^+ ions dominates for both electron capture and ionization channels at all energies, whereas for N^+ ions, the N_2^+ formation dominates for electron capture and the dissociative processes for ionization channels. The energy distribution of the fragment products at 20 and 100 keV have also been measured for the first time using the TOF method. These cross sections are useful in the simulation of energetic ions and atoms interacting with Titan's N_2 -rich atmosphere. Titan resides primarily within Saturn's magnetosphere where H^+ and N^+ ions are the major ions present along its orbit. It is found that the neutralization of these ions by charge exchange does not occur efficiently above Titan's exobase, so energetic particles with large gyroradii penetrate primarily as ions. The ionization rate and energy deposition in Titan's atmosphere by the energetic H^+ ions observed by the Voyager spacecraft are explained with the help of the present measurements. *INDEX TERMS:* 0343 Atmospheric Composition and Structure: Planetary atmospheres (5405, 5407, 5409, 5704, 5705, 5707); 2116 Interplanetary Physics: Energetic particles, planetary; 2423 Ionosphere: Ionization mechanisms; 2151 Interplanetary Physics: Neutral particles; *KEYWORDS:* Dissociation, nitrogen, capture, ionization, Titan, Saturn

Citation: Luna, H., M. Michael, M. B. Shah, R. E. Johnson, C. J. Latimer, and J. W. McConkey, Dissociation of N_2 in capture and ionization collisions with fast H^+ and N^+ ions and modeling of positive ion formation in the Titan atmosphere, *J. Geophys. Res.*, 108(E4), 5033, doi:10.1029/2002JE001950, 2003.

1. Introduction

[2] In this paper ionization and charge exchange cross sections are measured for H^+ and N^+ on N_2 in the energy range 10–100 keV. These cross sections are of interest at Titan, the largest moon of Saturn and the second largest moon in the solar system. Discovered by Christiaan Huygens in 1655, Titan has long been known to have a substantial atmosphere. Although its radius (2575 km) is about 40% of the Earth's radius, Titan has an atmosphere with a column density (number of molecules per unit area) that is more than an order of magnitude larger than that at Earth. Like the Earth, Titan's atmosphere near the surface is dominated by molecular nitrogen. However, nitrogen is about 97% of Titan's atmosphere with methane and other hydrocarbons making up the rest. Because of this composition, Titan's atmosphere is often thought to resemble a primordial atmosphere on Earth. Titan's atmosphere is also

unusually large due to its much smaller gravity. That is, the exobase altitude, the altitude above which escape occurs and below which the atmosphere is collisional, is about 60% of the planet's radius (~ 1500 km) whereas at the Earth it is $\sim 6\%$. Determining the origin and survival of this remarkable atmosphere is one of the principal goals of the Cassini Spacecraft, which will reach Saturn in 2004. It will launch a probe into Titan's atmosphere and also sense it remotely on numerous flybys.

[3] Titan orbits Saturn at a distance of $20.6 R_s$ [Saturn Radius (R_s) ~ 60268 km], which is inside Saturn's magnetosphere. The major magnetospheric ions near the orbit of Titan are H^+ , N^+ and, possibly, O^+ . As it is far from Saturn, Titan occasionally orbits outside of Saturn's magnetosphere and is in direct contact with the solar wind. This occurs when the solar wind pressure is high enough to significantly compress Saturn's magnetosphere. Because Titan does not appear to have an intrinsic magnetic field, magnetospheric or solar wind ions may penetrate into Titan's upper atmosphere depending on the induced local fields [Brecht *et al.*, 2000]. The processes measured here, charge exchange and ionization, are important when these ions interact with neutrals in the extended regions of the atmosphere called the atmospheric corona. The charge exchange reaction produces a fast neutral that is unaffected by the local fields and can directly penetrate into the atmosphere making collisions with the atmospheric neutrals. These processes

¹Department of Pure and Applied Physics, Queen's University Belfast, Belfast, United Kingdom.

²Department of Engineering Physics, University of Virginia, Charlottesville, Virginia, USA.

³School of Physical Sciences, University of Windsor, Windsor, Ontario, Canada.

can produce heating, collisional ejection of atoms and molecules (atmospheric sputtering), and expansion of the corona [Johnson, 1990, 1994]. New ions produced by the local fields contributing to mass loading and the induced fields near Titan [Brecht *et al.*, 2000]. The accelerated ions can also re-impact the atmosphere, in a feedback process, or can be swept away contributing to loss of atmosphere.

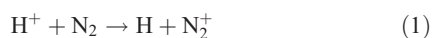
[4] The interaction between Saturn's magnetospheric plasma and the atmosphere of Titan is complex, but has been studied by a number of groups [e.g., Kivelson and Russell, 1983; Cravens *et al.*, 1998; Ledvina and Cravens, 1998; Lammer *et al.*, 1998; Kabin *et al.*, 2000; Brecht *et al.*, 2000; Chiu *et al.*, 2001; Nagy *et al.*, 2001; Kopp and Ip, 2001]. One of the largest uncertainties in these studies is the fraction of the incident plasma energy that is deposited in the atmosphere. The efficiency of these processes depends to first order on position of the ionopause, roughly the altitude where the incident plasma pressure is balanced by the ionospheric pressure. At Titan, the altitude of the nominal ionopause is uncertain with estimates of ~ 1900 km [Nagy and Cravens, 1998] to ~ 1200 km [Ip, 1990]. The latter is ~ 300 km below the exobase, which would imply most ions would be able to penetrate into Titan's atmosphere.

[5] The modeling of the interaction region also depends on the availability of high quality ion and electron impact cross sections. N₂ is the major species in Titan's atmosphere up to an altitude of 1700 km (~ 200 km above the exobase) with methane dominant above ~ 2500 km and H₂, H and N dominant at higher altitudes [Nagy and Cravens, 1998; Keller *et al.*, 1998]. Therefore, in describing Titan's interaction with magnetospheric or solar wind ions, cross sections with N₂ as the target are the most important. In the present paper cross sections for charge exchange and ionization of N₂ by H⁺ and N⁺ ions are reported. The energies of interest at Titan are ~ 1 keV to ~ 1 MeV. However, when Titan is within Saturn's magnetosphere, which is the case most of the time, the energy flux is likely carried by the 10–100 keV ions, as was found to be the case at the large moons of Jupiter by the Galileo spacecraft [Cooper *et al.*, 2001]. Since heating and atmospheric escape at Titan also depend on the fragmentation produced, dissociation cross sections and fragment energy spectra are also measured.

2. Cross Sections Measured

[6] We have used time of flight (TOF) coincidence counting techniques to measure the following individual dissociative and nondissociative cross sections of N₂ in collision with H⁺ and N⁺ ions over an energy range 10 to 100 keV (H⁺ projectile is used for illustrative purposes).

[7] Capture processes were measured for the nondissociative collisions



leading to N₂⁺ formation, for dissociative collisions

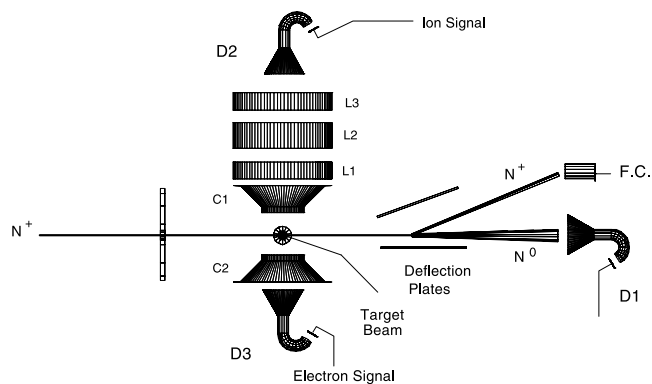
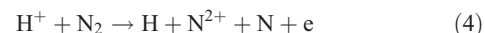


Figure 1. Schematic diagram of the apparatus.

leading to N⁺ + N formation, and for dissociative transfer ionization (TI) collisions

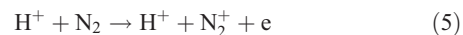


leading to N⁺ + N⁺ pair formation, and

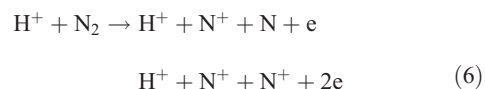


leading to N²⁺ formation.

[8] The ionization cross sections were measured for the nondissociative collisions



leading to N₂⁺ formation, the total N⁺ ion production in dissociative collisions



leading to N⁺ + N and N⁺ + N⁺ pair formation together with the dissociative collisions,



leading to N²⁺ formation.

[9] For N⁺ incident ions, further channels involving projectile electron loss collisions are possible but these were not considered in the present investigation. In the dissociative process the fragment energy spectra have also been measured.

3. Experiment

[10] Our well proven crossed beam TOF coincidence counting technique [McCartney *et al.*, 1999; McGrath *et al.*, 2001] have been used to measure individual cross sections of the many fragmentation channels of N₂ which arise during ionization and electron capture collisions with fast ions. Figure 1 shows the experimental setup. A primary beam of momentum analyzed H⁺ or N⁺ ions of selected energy within the range 10–100 keV was arranged to intersect at right angles a target beam of N₂ molecules

inside a high vacuum chamber. The main beam and its fast products were separated by deflection in a strong DC electrostatic field produced across a pair of deflection plates placed beyond the interaction region. The neutral products, resulting from electron capture collisions, were detected by the on axis channeltron detector, D₁, and the main beam was collected by the Faraday cup FC.

[11] The target beam was formed inside a separate differentially pumped chamber by allowing the target gas to effuse from a bunch of 1 mm diameter hypodermic needles set within a 4 mm diameter tube. The gas jet traveled a distance of 70 mm before entering the main chamber through a 4 mm diameter collimator placed 20 mm away from the interaction region. This arrangement provided a well-confined target beam in the interaction region giving only a small amount of pressure rise in the main chamber when target gas was introduced. This was of particular importance in measurements involving electron capture as contributions to the fast projectile signal were supplemented by collisions with the background gas along the length traveled by the beam in the main chamber. To alleviate this problem, a set of three deflecting plates (not shown for clarity) were used to wiggle the main beam just before the interaction region and remove any capture contributions from the beam received upstream of the plates. The downstream main beam charge analysis deflection plates were placed as close to the interaction region as possible. In this way the undesirable contribution was reduced to a manageable level. The main chamber base pressure was about 1.0×10^{-7} mbar and this increased to around 1.5×10^{-7} mbar when the target gas was introduced.

[12] The ions and electrons formed from the target gas in the crossed beam intersection region were collected by a transverse electric field applied across the intersection region and separately counted by the channeltron detectors D₂ and D₃, respectively. In the present measurements great care was taken to ensure that the target fragment products N⁺ and N²⁺ carrying a range of dissociation energies were collected with equal and with high efficiencies. This was achieved by using a combination of large collection areas and high extraction fields. The conical shaped extraction electrodes, C1 and C2 with openings of 15 mm in diameter, placed 8 mm on either side of the interaction region collected essentially all of the target products formed across the 4 mm diameter target beam when 300 volts were applied across the cones. The electrostatic fields produced were mainly confined around the interaction region. These fields did not deflect the projectile beam by an appreciable amount even at our lowest incident energy of 10 keV. High transparency grids set within the openings in C1 and C2 permitted the target products to go past the electrodes and onto the detectors D₂ and D₃. These detectors had an entrance diameter of 20 mm each. The various dissociative and nondissociative target products were separated from one another according to their charge/mass ratios by the use of TOF techniques. For this purpose, the time to amplitude converter (TAC) unit was supplied with stop pulses derived from the detector D₂ and start pulses from either the detector D₁ when carrying out measurements on the electron capture channels or the detector D₃ when carrying out measurements on the ionization channels. We found it necessary to place D₂ at a distance of 40 mm away from the intersection

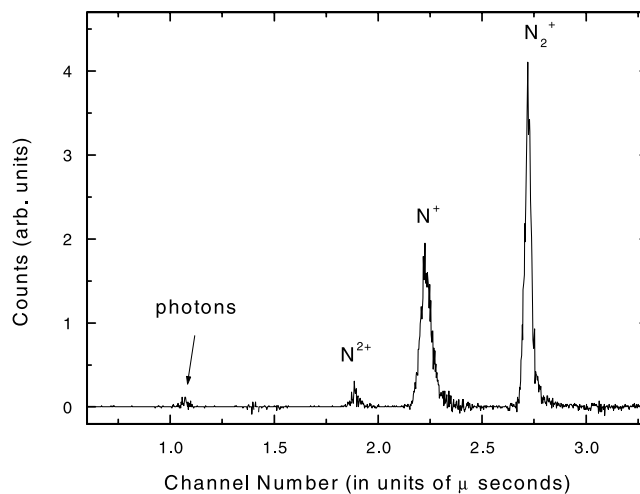


Figure 2. TOF spectrum of N₂ target products formed during electron capture collisions with 70 keV H⁺ incident ions. Despite suffering reductions from acceptance angles and detection efficiencies, the photon peak indicates substantial presence of radiative decay processes.

region and to focus the extracted target products onto the detector before the measured TOF spectra provided sufficient resolution to adequately separate the various target products from one another. An electrostatic lens system, comprising of L1, L2 and L3 operated as an iso-lens combination, was used to focus the extracted slow ion products. A typical TOF spectrum for N₂ involving electron capture collisions by 70 keV H⁺ is shown in Figure 2. As seen all the target product peaks are well resolved from one another. It is worth noting that the N₂⁺ peak corresponding to the pure capture channel (1) is the most dominant for 70 keV H⁺ collision. The N⁺ peak resulting from the dissociative channels (2) and (3) is broadened due to the dissociation energies. When the integrated peak areas are considered, the N⁺ peak is smaller than the N₂⁺ peak by only a small factor.

3.1. Cross Section Measurements and Normalization

[13] From the TOF spectra of the type shown in Figure 2, relative cross sections for individual channels were obtained by integrating the areas under the appropriate peaks. Thus, from the spectra obtained with the start pulses derived from detector D₁ and the stop pulses from detector D₂, the areas under the N₂⁺ and N²⁺ peaks gave relative cross sections for the nondissociative capture channel (1) and the dissociative TI channel (4), respectively. Similarly, the area under the N⁺ peak gave relative cross sections for the sum of the dissociative capture channels (2) + (3).

[14] From the spectra measured with start pulses supplied from the electron detector D₃ and the stop pulses from detector D₂, relative cross sections for channels involving the production of electrons were obtained. With additional refinement of gating the TAC unit with pulses from the fast detector D₁, the electron production channels were separated further. For example, when the TAC unit Gate received pulses from D₁ simultaneously with the start and the stop pulses (triple coincidence mode), the areas under the N⁺ and N²⁺ peaks provided relative cross sections for

Table 1. Dissociative and Nondissociative Cross Sections for the Capture and Ionization Channels (1) to (7) of N₂ in Collision With H⁺ Expressed in Units of 10⁻¹⁷ cm²

Energy, keV	Channel						
	(1)	(2)	(3)	(4)	(5)	(6)	(7)
10	84 ± 7	11.3 ± 1.3	5.4 ± 0.7	0.27 ± 0.02	11.2 ± 1.2	8.7 ± 1.1	0.27 ± 0.04
20	58 ± 5	10.5 ± 1.2	8.3 ± 1.1	0.63 ± 0.05	17.7 ± 1.9	12.7 ± 1.4	0.53 ± 0.07
30	41 ± 3	8.6 ± 1.0	8.6 ± 1.1	0.94 ± 0.08	23 ± 3	14.2 ± 1.5	0.9 ± 0.1
40	31.2 ± 2.5	7.4 ± 0.8	8.0 ± 1.0	0.98 ± 0.08	30 ± 3	14.7 ± 1.6	1.1 ± 0.1
50	22.5 ± 1.8	6.2 ± 0.7	6.6 ± 0.9	0.98 ± 0.08	31 ± 3	14.7 ± 1.5	0.9 ± 0.1
60	17.9 ± 1.4	5.6 ± 0.6	5.6 ± 0.7	0.84 ± 0.07	35 ± 3	15.3 ± 1.6	1.1 ± 0.1
70	13.5 ± 1.1	4.8 ± 0.5	4.6 ± 0.6	0.65 ± 0.05	35 ± 3	14.3 ± 1.5	1.1 ± 0.1
80	10.5 ± 0.8	3.7 ± 0.5	3.8 ± 0.5	0.52 ± 0.04	35 ± 3	13.7 ± 1.4	1.0 ± 0.1
90	8.6 ± 0.7	3.1 ± 0.4	2.9 ± 0.4	0.45 ± 0.04	37 ± 3	14.5 ± 1.6	0.9 ± 0.1
100	6.8 ± 0.5	2.3 ± 0.3	2.3 ± 0.3	0.39 ± 0.03	35 ± 3	13.3 ± 1.4	1.0 ± 0.1

the individual dissociative TI channels (3) and (4), respectively. In the same way, when the TAC unit Gate was set to reject conversions when pulses from D₁ were present (anti-coincidence mode), the areas under the N₂⁺, N⁺ and N²⁺ peaks gave the fully resolved relative cross sections for the nondissociative ionization channel (5), and the dissociative ionization channels (6) and (7), respectively.

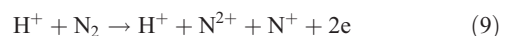
[15] Our measured relative cross sections for the capture channels involving detectors D₁ and D₂ could be assigned absolute values from the equation

$$\sigma_c = kS_c/(\varepsilon_1\varepsilon_2) \quad (8)$$

where S_c is the peak area obtained from the measured TOF spectrum per unit projectile current and unit pressure, ε₁ and ε₂ are, respectively, the detection efficiencies of the detectors D₁ and D₂ and k incorporates target thickness (length × number density) and the pressure and the current converter factors. Both the current and the pressure monitor were routed through voltage to frequency converters to minimize errors from these sources.

[16] In order to assign absolute values to σ_c, it was necessary to determine the product k/(ε₁ε₂) in equation (8) by normalization to known cross sections. In the present work we used the well established total one electron capture cross sections of *Stier and Barnett* [1956] for proton impact which are believed to be accurate to within 5%. We added our relative cross sections for the individual channels (1), (2), (3) and (4) for this purpose and compared them with the values of *Stier and Barnett* [1956] over an energy range 10–30 keV where the capture cross sections remain high.

[17] The cross sections for the ionization channels measured with the electron detector D₃, were obtained from a similar equation that included the efficiency, ε₃, of the electron detector. This efficiency was determined in the following manner. The TI channel (4) recorded during the capture measurements involved the detectors D₁ and D₂, and during the ionization measurements in the triple coincidence mode involved all three detectors. The ratio for channel (4) from the two measurements then directly provided the required value for ε₃. It should be noted that



would also contribute to channel (4), but since removal of three target electrons is involved, these contributions are taken to be insignificant in the present energy range.

[18] Cross sections for channels (1) to (7) for N⁺ impact were also measured by replacing the H⁺ beam with a beam of N⁺ ions.

4. Results

[19] Our cross sections for channels (1) to (7) in collisions with H⁺ and N⁺ measured over the energy range 10–100 keV are given in Tables 1 and 2, respectively. The uncertainties associated with individual cross sections reflect the degree of reproducibility of the values in terms of the various experimental parameters and statistical fluctuations. Channel (2) could not be measured directly and the uncertainty for (2) includes the additional error involved in subtracting contributions of channel (3) from the measured

Table 2. Dissociative and Nondissociative Cross Sections for the Capture and Ionization Channels (1) to (7) of N₂ in Collision With N⁺ Expressed in Units of 10⁻¹⁷ cm²

Energy, keV	Channel						
	(1)	(2)	(3)	(4)	(5)	(6)	(7)
10	65 ± 5	11.1 ± 1.4	2.3 ± 0.3	0.1 ± 0.01	6.5 ± 0.8	17.3 ± 2.0	1.2 ± 0.2
20	75 ± 5	16.6 ± 1.8	4.5 ± 0.6	0.35 ± 0.02	8.8 ± 1.1	25.9 ± 3.0	2.9 ± 0.4
30	73 ± 5	16.5 ± 1.7	5.9 ± 0.8	0.68 ± 0.05	7.9 ± 1.0	28.7 ± 3.3	4.1 ± 0.5
40	76 ± 5	17.4 ± 1.5	6.8 ± 0.9	0.9 ± 0.1	9.6 ± 1.0	35 ± 3	6.3 ± 0.8
50	76 ± 5	18.4 ± 1.5	7.4 ± 1.0	1.1 ± 0.1	9.4 ± 1.0	39 ± 4	8.1 ± 1.1
60	75 ± 5	17.3 ± 1.5	8.6 ± 1.1	1.2 ± 0.1	10.3 ± 1.1	43 ± 4	9.1 ± 1.1
70	72 ± 5	16.5 ± 1.4	9.4 ± 1.2	1.3 ± 0.1	10.5 ± 1.1	43 ± 4	10.8 ± 1.4
80	69 ± 5	16.4 ± 1.4	10.0 ± 1.3	1.5 ± 0.1	10.8 ± 1.1	46 ± 4	12.4 ± 1.6
90	65 ± 5	15.2 ± 1.4	10.3 ± 1.3	1.7 ± 0.1	11.7 ± 1.2	48 ± 4	12.8 ± 1.7
100	61 ± 4	14.1 ± 1.3	10.4 ± 1.3	1.7 ± 0.1	10.9 ± 1.2	47 ± 4	13.7 ± 1.8

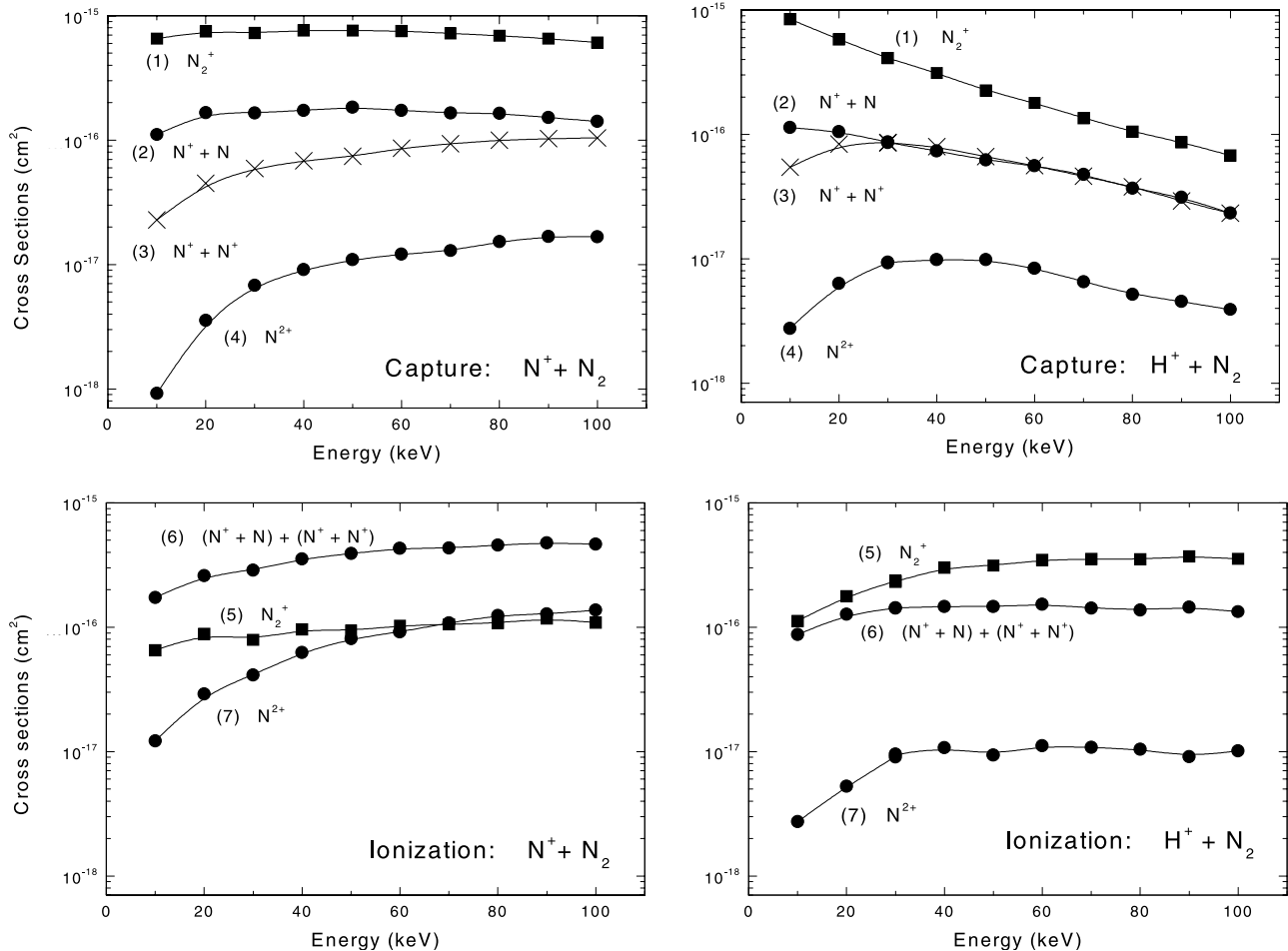


Figure 3. Dissociative and nondissociative cross sections for channels (1) to (7) in collisions with H^+ and N^+ ions. Capture cross sections are shown in the top set and ionization cross sections in the bottom set of diagrams.

sum (2) + (3). All the cross sections are subject to a further uncertainty in the absolute values resulting from the use of our normalization procedure. This is 8% for channels (1) and (4) and 13% for the remaining channels. These remaining channels used the additional electron detector D_3 and its efficiency determination via channel (4), involved weak signals. These individual cross sections for both H^+ and N^+ impact are shown in Figure 3. For clarity, the cross sections are separated into groups containing channels that result from collisions involving capture (top half) and pure ionization (bottom half).

[20] In the case of proton impact, the nondissociative channels leading to N_2^+ formation dominate for both the electron capture and the ionization channels at all energies within the present range. At 100 keV, the ionization channel (5) is the largest while at 10 keV it is the capture channel (1) that is the largest. However, it is also seen that the dissociation channel leading to the formation of atomic neutral and ionized fragments is not significantly smaller. For capture, the dissociative channels (2) for $N^+ + N$ formation and (3) for $N^+ + N^+$ formation are identical in magnitude over the present energy range except at our lowest energy. When contributions from (2) and (3) are combined, the total N^+ production channel is only about a factor of 1.5 smaller than

the N_2^+ production channel (1) at 100 keV and about a factor of 8 smaller at 10 keV. For ionization, the $N^+ + N$ and the $N^+ + N^+$ channels could not be separated. For N^{2+} formation, the channel (4) for capture and channel (7) for ionization, are between one and two orders of magnitude smaller than their respective channels (1) and (5) for N_2^+ formation.

[21] Cross sections for incident N^+ ions show rather interesting differences from those seen with H^+ ions. Whereas for capture, channel (1) for N_2^+ formation is the largest over the whole present range, for ionization it is the dissociative channels that are the largest. Also, the ionization channel (7) for N^{2+} formation is comparatively large (over an order of magnitude larger than for H^+ at same impact energies) and indeed greater than the nondissociative channel (5) at our highest energies.

[22] In order to provide deeper insights into the dissociative processes, we have carried out energy distribution measurements of the fragment products for H^+ and N^+ impact at incident energies of 20 and 100 keV. As seen from Figure 4, the distributions for the $N^+ + N^+$ pair production and for the sum $(N^+ + N) + (N^+ + N^+)$ production have almost identical shapes at 20 and 100 keV for H^+ but markedly different shapes for N^+ impact. The present H^+ induced $N^+ + N^+$ distributions show features

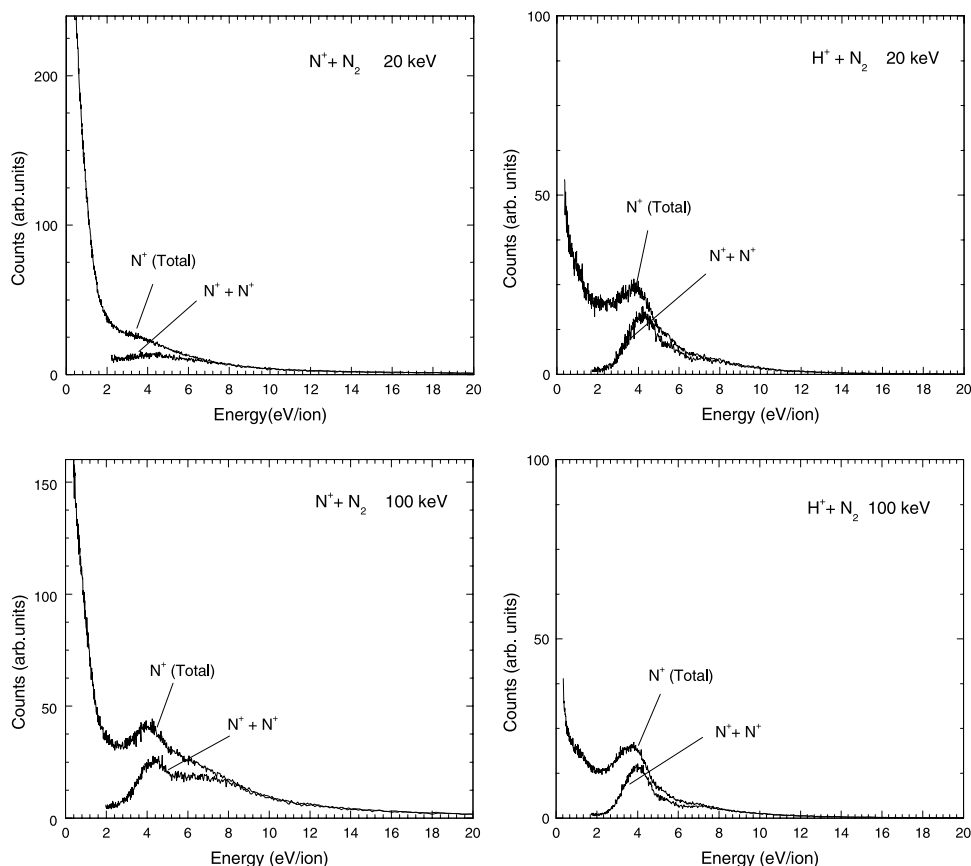


Figure 4. Energy distributions of N^+ fragment products emitted at 90° during collisions of H^+ and N^+ incident ions on N_2 . Curves labeled $N^+ + N^+$ show energy distributions of events leading to $N^+ - N^+$ pairs production and curves labeled N^+ show energy distributions of all events leading to N^+ production. Contributions from both capture and ionization channels are included.

which are broadly in agreement with the 1 MeV measurements of *Edwards and Wood* [1982] and the 15 keV measurements of *Yousif et al.* [1990]. The dominant peak for the pair production in their spectra appear at 3.9 and 3.8 eV, respectively, compared to at around 4.2 eV in the present measurement. The previous two measurements also show minor peaks appearing at 5.1 eV and at about 7.5 eV which are confirmed in the present measurements when the 100 keV H^+ distribution is examined closely. These investigators used electrostatic energy analyzers to measure their energy distributions whereas the present work used TOF methods. In the measurements, the extraction cones C_1 and C_2 and the elements L_1 , L_2 and L_3 of the lens assembly were grounded. The insides of all these electrodes and other components surrounding the interaction regions were coated with a compound of graphite to reduce effects of contact potentials influencing the energy distributions. The main beam was pulsed with a width of 100 nsec and pulse separation of 50 μ sec. The start pulse to the TAC unit was supplied from the main beam pulser unit and the stop pulse from the detector D_2 . For the $N^+ + N^+$ pair production measurements, the output from the detector D_3 was supplied to the Gate input of the TAC unit. The recorded TOF spectra were then transformed into energy spectra.

[23] It should be pointed out that the energy distributions obtained with the TOF method used in the present work is

sensitive to the existence of long-lived intermediate states. Break-up decay times increase the measured flight times and, thus, falsely attribute lower energies to the fragments. Our large collection geometry optimized for the total cross section measurements would particularly suffer from long-lived intermediate states as our geometry can accommodate life times approaching 20 μ sec. However, the electrostatic energy analyzers used by *Edwards and Wood* [1982] and *Yousif et al.* [1990] are insensitive to the presence of long-lived states.

[24] Our measured energy spectra for all events leading to N^+ production are also shown in Figure 4. The distributions show the presence of a peak at 3.8 eV which is also seen in the 15 keV measurement of *Yousif et al.* [1990] but at a position of 3.5 eV. The later authors also show a well-defined low energy peak centered at 1.0 eV. The present distributions for H^+ show a point of inflection at this energy and show that in fact, there are a substantial number of N^+ fragments that have much lower apparent energies. *Crowe and McConkey* [1975], in search of near zero energy N^{2+} fragments in collision with electrons, found that the incident beam space charge was affecting the detection of the near zero energy fragments. However, even though they reduced their beam intensity by a factor of ten, they still did not find any near zero energy N^{2+} , but near zero energy N^+ and N_2^+ were readily recorded. Because of the large collection

Table 3. Ratios of Events Leading to the N⁺ + N⁺ Pair Production to Total Events Leading to N⁺ Production Obtained by Integrating the Energy Distribution Spectra Shown in Figure 4

Energy, keV	N ⁺ Impact	H ⁺ Impact
20	0.28	0.38
100	0.43	0.42

efficiencies in the present work, beam currents used were about 10⁻¹⁰ DC equivalent. However, as the main beam was pulsed, any beam related space charge disappeared soon after the 100 nsec beam pulse exited the interaction region.

[25] Inspection of the N⁺ + N⁺ pair production in Figure 4 for 100 keV incident H⁺ and N⁺ ions reveals that for N⁺ impact many events with energies much higher than the pronounced 4.2 eV peak are present in comparison with H⁺ impact. In contrast at 20 keV the N⁺ incident ions produce, negligible numbers of N⁺ + N⁺ pairs. Clearly, the equivalent incident energy of 1.4 keV/u is too small to transfer large amounts of energy to two target electrons efficiently. The N⁺ target fragment ions with low apparent energies, not withstanding the influence of large life times elaborated above, also seem to be populated in higher numbers for N⁺ projectiles at both 20 and 100 keV. Table 3 gives the ratio for the N⁺ + N⁺ pair production over the total events for N⁺ production (obtained by integrating the N⁺ + N⁺ energy distributions and the N⁺ energy distributions of Figure 4) for the two projectiles at the incident energies of 20 and 100 keV. The spectra in Figure 4 include contributions from the capture as well as the ionization processes.

4.1. Comparison With Previous Work

[26] It is interesting to compare our present cross section measurements with previous work. Only measurements with H⁺ projectiles are available where serious attempts were made to separate the various target product species. The total cross sections of *Browning and Gilbody* [1968] resulting from capture and ionization collision are compared with our capture and ionization summed cross sections for N₂⁺, N⁺ and N²⁺ production, in Figure 5. As can be seen, the agreement with the two sets of data is excellent for the abundant N₂⁺ and N⁺ species, and just differs by 20% for N²⁺. The cross sections for N⁺ + N⁺ pair production at 20 keV of *Yousif et al.* [1990] obtained by integrating their angular measurements are also included. We were unable to separate our N⁺ + N and the N⁺ + N⁺ channels for ionization, and thus, in this case we do not include our data for comparison.

5. Titan Atmosphere

[27] Our H⁺ and N⁺ measurements given in Table 1 provide details of the dissociative and nondissociative collisions made by the energetic solar wind and trapped magnetospheric ions with Titan's atmosphere. We provide total cross sections, cross sections for dissociation, and fragment energy spectra when dissociation occurs. Previous low energy measurements of N⁺ on N₂ have been restricted to the production of total positive target ions. In Figure 6 we compare our total target positive ion production cross sections with the compilation of *Phelps* [1991]. It is seen

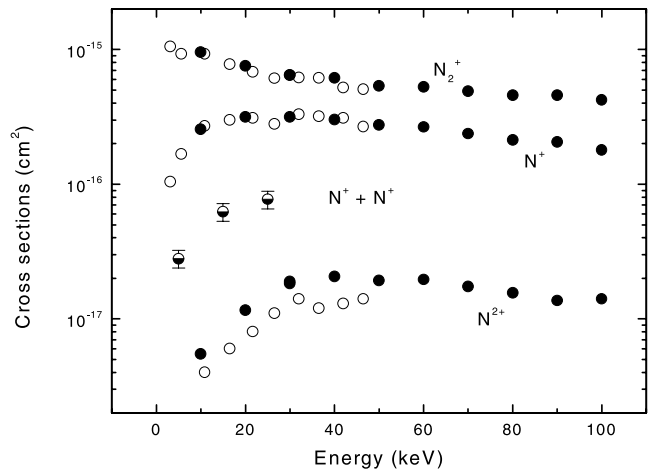


Figure 5. Comparison for the total production of N₂⁺, N⁺, N⁺ + N⁺ pair and N²⁺ ions with previous measurements in collisions of H⁺ with N₂. Filled circle, present data; open circles, *Browning and Gilbody* [1968]; bottom filled circles, *Yousif et al.* [1990].

that the previous measurements agree very well with our totals. The higher energy data of the *Phelps* [1991] compilation mostly include the measurements of *Stebbins et al.* [1963], which the authors attribute to one electron capture. However, on close examination of the *Stebbins et al.* [1963] paper, it is clear that the authors measure the production of positive ion current. Thus their cross sections determine the total production of positive ions. The data of *Stebbins et al.* [1963] were normalized, as in the present case, to the one electron capture cross sections of *Stier and Barnett* [1956]. It should be noted that Phelps refers to the compilation data as being due to one electron capture cross sections for N₂⁺ formation (i.e. channel 1). While this is true at low energies much below the maximum of 10 keV, our data show that at 10 keV dissociative capture and ionization processes make up about 30% of total cross sections.

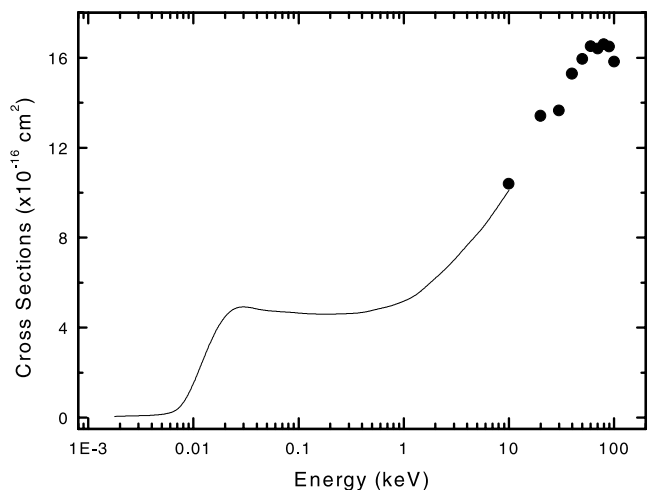


Figure 6. Comparison of present cross sections for total positive ion production with previous measurements in collisions of N⁺ with N₂. Filled circle, present data; solid line, compilation of experimental data by *Phelps* [1991].

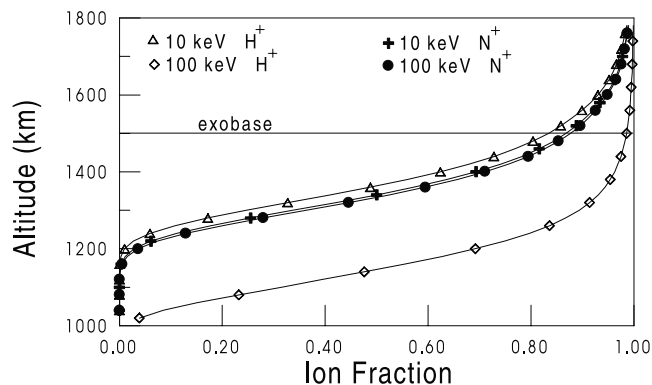


Figure 7. Fraction of incident ions that are not neutralized as a function of altitude above the surface of Titan calculated using charge exchange cross sections in Figure 3 and N₂ densities from Keller *et al.* [1998]. The exobase is marked (the altitude above which collisions between atmospheric molecules become improbable and escape can occur).

[28] Since Titan has an extended atmosphere and no intrinsic magnetic field, the magnetospheric and solar wind ions can penetrate the exobase causing heating of the thermosphere and ejection of atoms and molecules as discussed. Ionization, typically by solar photons and plasma electrons, results in the pick-up of newly formed ions and in induced fields that partially deflect the plasma flow [Brecht *et al.*, 2000]. Whereas the surface temperature is estimated as 94 K, the temperature at the exobase has been given as 186 K [Smith *et al.*, 1982; Lindal *et al.*, 1983] but must depend on the plasma heating rate. If the ionopause is ~ 1200 km, as suggested in some models then the full flux of low and high energy particles will contribute to heating of the atmosphere near the exobase. However, most models indicate that the induced fields begin to modify the ion flow above the exobase, ~ 1900 km. In that case the ability of energetic ions to penetrate to the exobase and heat the atmosphere depends on both the radius of their gyromotion about the local field lines and on where they experience charge exchange. That is, if the scale of the gyromotion is comparable to the radius of the obstacle, the ions are not deflected efficiently by the induced fields and can still penetrate into Titan's atmosphere. For the energy range considered here the gyroradii for H⁺ and N⁺ are of the order of ~ 1 to 3 and ~ 4 to 12 Titan radii, respectively, when Saturn's magnetosphere is not compressed significantly. On the other hand, once the incident ions neutralize they are not affected by the local fields, again allowing them to penetrate the exobase.

[29] Here we use the upper atmosphere model of Keller *et al.* [1998] in which the number density and column density of N₂ at the exobase are about 2.7×10^7 N₂/cm³ and 2.3×10^{14} N₂/cm², respectively. For the ion energies measured we give in Figure 7 the fraction of the incident ions that are not neutralized versus depth into Titan's atmosphere. Based on the cross sections measured here, about 20% of the N⁺ and the protons in the 10 keV energy range are neutralized before reaching the exobase but almost all (98%) of the 100 keV protons that reach the exobase penetrate as ions. In the absence of deflection by the fields or scattering, most of the

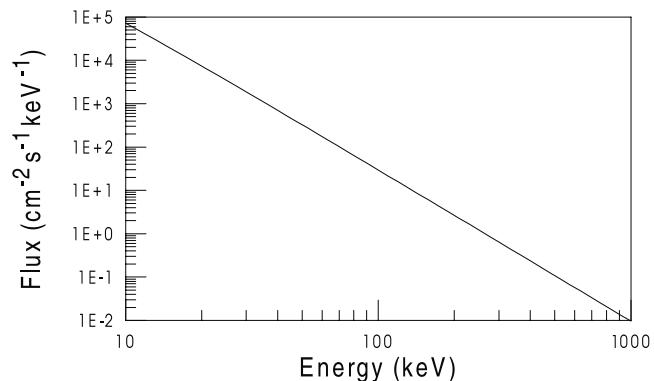


Figure 8. Flux of protons observed by Voyager 1 at Titan's orbital radius [Schardt *et al.*, 1984].

N⁺ and the protons ~ 10 keV are neutralized by an altitude ~ 1200 km above the surface of Titan, whereas the 100 keV protons are not mostly neutralized until ~ 1000 km.

[30] The penetrating ions and neutrals produce additional ionizations as well as heating. Any ions newly formed can be accelerated by the local fields and penetrate the atmosphere increasing the heating. The plasma flow speed inside Saturn's magnetosphere at Titan's radius results in a "thermal" component of H⁺ and N⁺ of energies ~ 0.2 keV and ~ 3 keV, respectively, energies somewhat lower than those studied here. Surprisingly, the N⁺ flux greater than ~ 10 keV was found to be small at the time of the Voyager flybys but a significant energetic H⁺ flux was seen. We expect a detection of the energetic N⁺ by the Cassini spacecraft. In Figure 8 is shown an extrapolation of the H⁺ ion flux for the energy range of interest (>10 keV). This flux is multiplied by the N₂ density and by the cross sections for ionization and charge exchange extrapolated from our data to higher energies. This gives the energetic proton contribution to the ion formation rate versus depth into Titan's atmosphere shown in Figure 9. These ionizations can lead to emissions

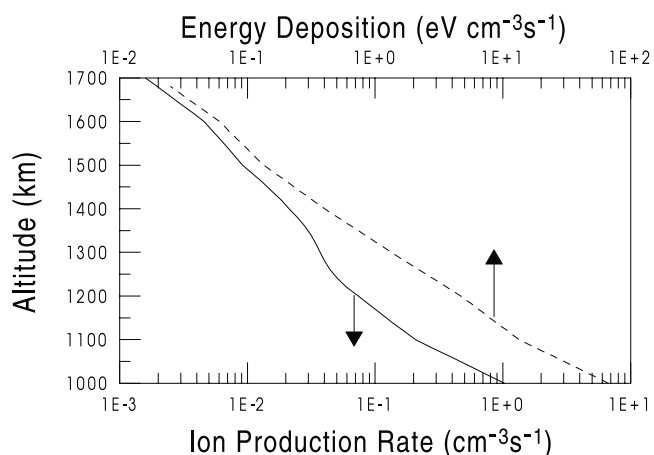


Figure 9. Ion production rate (solid curve) and energy deposition rate (dashed curve) by the proton interaction in the atmosphere of Titan. In the ionization rate the charge exchange cycle is ignored so that charge exchange contributes only once. The energy deposition is obtained using the TRIM values for the electronic stopping power.

and chemistry during the recombination process, which we will describe separately. In addition, depending on the local fields, the newly formed ions can be accelerated, as discussed above. At distances 400 km above the exobase the N⁺ and N₂⁺ are accelerated to ~3 keV and ~6 keV, respectively, with gradually decreasing energies for ions formed at lower altitudes where the induced fields alter the flow [Brecht *et al.*, 2000].

[31] The energetic protons carry an energy flux $\sim 5 \times 10^9$ eV/cm²/s which is comparable with that due to the energetic magnetospheric electrons and to the lower energy “thermal” plasma, while solar UV photons carry an energy flux of about a factor of 4 larger, $\sim 2 \times 10^{10}$ eV/cm²/s. Since the ionizations and excitations by incident ions and photons can involve rather different states, describing the effect of the energetic protons is important. For illustrative purposes we also multiplied the energetic proton flux by the electronic stopping power to obtain the energy deposition versus depth into the atmosphere. This result is also given in Figure 9. In the later we use an estimate of the stopping power from Zeigler *et al.* [1985]. Ignoring the contribution from freshly produced ions, the heating rate and chemistry induced near the exobase will be smaller than that by the UV photons but contribute at greater depths than the lower energy component of the plasma [Lammer *et al.*, 1998]. The N₂⁺ ion production rate by the solar photons is maximum at about 1000 km [Keller *et al.*, 1992] where the direct ionization by energetic protons is about an order of magnitude less (using the energy deposition divided by the W-value (~30 eV/ionization) the net ionization by the protons is approximately twice in Figure 9). Keller *et al.* [1992] used the solar photon flux (0.5 Å to 1310 Å) by scaling the solar minimum reference spectrum of Hinteregger and Fukui [1981] to obtain an EUV flux representative of the conditions at the time of the Voyager 1 encounter.

[32] The fragment energies and cross sections measured here are not only diagnostic of the collision processes but can be used to determine the loss of atmosphere by impacting energetic ions [Johnson, 1994; Lammer *et al.*, 1998]. A nitrogen atom produced by a dissociation process at the exobase requires only ~0.34 eV to escape Titan’s gravity. Therefore, the neutral fragments, which must have energies comparable to the ion fragments in Figure 4, or ion fragments that immediately charge exchange, can readily escape from Titan if their velocities are in the right direction. The correct modeling of the heating and the atmospheric loss requires the use of a Monte Carlo tracking of the fragments and the struck N₂ through the background gas [Shematovich *et al.*, 2001]. Such results will be separately investigated and the effect of the incident ions compared to other loss processes.

6. Conclusions

[33] We have carried out new measurements of the interaction of 10–100 keV H⁺ and N⁺ ions with N₂ and cross sections for ionization and charge exchange both with and without fragmentation of the target molecule, are reported. N₂⁺ is the dominant product for incident H⁺ but for incident N⁺, is only dominant for the charge exchange process. Dissociation dominates the ionization channel for incident N⁺. These cross sections are comparable to earlier

related measurements, and the total target ion production by incident N⁺ is found to fit smoothly onto the earlier measurements at lower energies. The latter were given as charge exchange cross sections but are in fact cross sections for total target ion production. In addition, we measured energy spectra of the fragment products which show that substantial numbers carry energies to escape Titan’s gravity if formed near the exobase.

[34] The data obtained here will be useful for modeling the chemistry, emissions and heating induced by magnetospheric or solar wind plasma bombardment of Titan’s atmosphere. According to Lammer and Bauer [1993], magnetospheric N⁺ and H⁺ and solar wind protons initiate the most efficient escape process for eroding Titan’s dense N₂ atmosphere, although this was questioned recently [Shematovich *et al.*, 2001]. Lammer *et al.* [1998] suggested that the dominant ~3 keV N⁺ ions deposit their energy below the exobase but did not describe the role of the more energetic ions, which carry a comparable energy flux. The cross-sections given here show that neutralization of the incident ions by charge exchange does not occur efficiently above the exobase, which is unlike what was found at Mars [Luhmann and Kozyra, 1991; Leblanc and Johnson, 2001]. Therefore, if the gyroradii and the induced fields are such that they can reach the exobase, the energetic particles penetrate predominantly as ions. Protons with energies ~10 to 100 keV penetrating into the atmosphere deposit most of their energy below the exobase whereas the heating near the exobase is likely due to lower energy N⁺ and H⁺ (M. Michael *et al.*, Plasma heating and sputtering of Titan’s atmosphere, manuscript in preparation, 2003). The energy deposited by these ions in Titan’s upper atmosphere raises the exobase temperature and expands the upper atmosphere [Shematovich *et al.*, 2001]. This can, in turn, increase the nonthermal escape rates and act as a mechanism to populate Saturn’s plasma torus. Brecht *et al.* [2000] point out that the gyroradii of the pick up ions are very important in the simulation of the Titan interaction with the magnetospheric flow. Since in the energy range of interest (10–100 keV), the gyroradii of H⁺ and N⁺ are comparable to or much larger than Titan’s radius, these ions should have access to Titan’s atmosphere. To correctly describe the flow of the magnetospheric ions into the atmosphere, a 3-dimensional multi-species model will be required. For such an elaborate model an accurate cross section database is also required.

[35] **Acknowledgments.** The authors would like to thank the Brazilian CNPq agency for providing funds to H. Luna for a one year’s postdoctoral visit to Belfast. MBS and CJL would like to acknowledge financial assistance from the UK EPSRC. JW McC thanks NSERC, Canada for financial support. The work at Virginia was supported by NASA’s Planetary Atmospheres Program.

References

- Brecht, S. H., J. G. Luhmann, and D. J. Larson, Simulation of the Saturnian magnetospheric interaction, *J. Geophys. Res.*, *105*, 13,119, 2000.
- Browning, R., and H. B. Gilbody, Fragmentation of molecular gases by 5–45 keV protons, *J. Phys. B At. Mol. Phys.*, *1*, 1149–1156, 1968.
- Chiu, W. T., H. C. Hsu, A. Kopp, and W. H. Ip, On ion outflows from Titan’s exosphere, *Geophys. Res. Lett.*, *28*, 3405, 2001.
- Cooper, J. F., R. E. Johnson, B. H. Mauk, H. B. Garret, and G. Neil, Energetic ion and electron irradiation of the icy Galilean Satellites, *Icarus*, *149*, 133, 2001.
- Cravens, T. E., C. J. Lindgren, and S. A. Ledvina, The two dimensional multifluid MHD model of Titan’s plasma environment, *Planet. Space Sci.*, *46*, 1193, 1998.

- Crowe, A., and J. W. McConkey, Dissociative ionization by electron impact, IV, Energy and angular distributions of N₂⁺ from N₂, *J. Phys. B At. Mol. Phys.*, **8**, 1765–1769, 1975.
- Edwards, A. K., and R. M. Wood, Dissociation of N₂⁺ ions into N⁺ fragments, *J. Chem. Phys.*, **76**, 2938–2942, 1982.
- Hinteregger, H. E., and K. Fukui, Observational reference and model data on solar EUV from measurements on AE-E, *Geophys. Res. Lett.*, **8**, 1147, 1981.
- Ip, W. H., Titan's upper atmosphere, *Astrophys. J.*, **362**, 354, 1990.
- Johnson, R. E., *Energetic Charged-Particle Interactions With Atmospheres and Surfaces*, Springer-Verlag, New York, 1990.
- Johnson, R. E., Plasma ion sputtering of an atmosphere, *Space Sci. Rev.*, **69**, 215, 1994.
- Kabin, K., P. L. Israelevich, A. I. Ershkovich, F. M. Neubauer, T. I. Gombosi, D. L. DeZeeuw, and K. G. Powell, Titan's magnetic wake: Atmospheric or magnetospheric interaction, *J. Geophys. Res.*, **105**, 10,761, 2000.
- Keller, C. N., T. E. Cravens, and L. Gan, A model of the ionosphere of Titan, *J. Geophys. Res.*, **97**, 12,117, 1992.
- Keller, C. N., V. G. Anicich, and T. E. Cravens, Model of Titan's ionosphere with detailed hydrocarbon ion chemistry, *Planet. Space Sci.*, **46**, 1149, 1998.
- Kivelson, M. G., and C. T. Russell, The interaction of flowing plasmas with planetary ionospheres: Titan – Venus comparison, *J. Geophys. Res.*, **88**, 49, 1983.
- Kopp, A., and W. H. Ip, Asymmetric mass loading effect at Titan's ionosphere, *J. Geophys. Res.*, **106**, 8323, 2001.
- Lammer, H., and S. J. Bauer, Atmospheric mass loss from Titan by sputtering, *Planet. Space Sci.*, **41**, 657, 1993.
- Lammer, H., W. Stumptner, and S. J. Bauer, Dynamic escape of H from Titan as consequence of sputtering induced heating, *Planet. Space Sci.*, **46**, 1207, 1998.
- Leblanc, F., and R. E. Johnson, Sputtering of the Martian atmosphere by solar wind pick-up ions, *Planet. Space Sci.*, **49**, 645, 2001.
- Ledvina, S. A., and T. E. Cravens, A three dimensional MHD model of plasma flow around Titan, *Planet. Space Sci.*, **46**, 1175, 1998.
- Lindal, G. F., G. E. Wood, H. B. Hotz, and D. N. Sweetnam, The atmosphere of Titan: An analysis of the Voyager 1 radio occultation measurements, *Icarus*, **53**, 348, 1983.
- Luhmann, J. G., and J. U. Kozyra, Dayside pick-up oxygen in precipitation at Venus and Mars: Spatial distribution, energy deposition and consequences, *J. Geophys. Res.*, **96**, 5457, 1991.
- McGrath, C., M. B. Shah, P. C. E. McCartney, and J. W. McConkey, H₂⁺ (20–100-keV) collisions with H: Dissociative and nondissociative capture and ionization and pure-H-target ionization, *Phys. Rev. A*, **64**, 062712, doi:10.1103/PhysRevA.64.062712, 2001.
- McCartney, P. C. E., C. McGrath, J. W. McConkey, M. B. Shah, and J. Geddes, Collisions of H₂⁺ with H: Individual fragmentation channels, *J. Phys. B At. Mol. Phys.*, **32**, 5103, 1999.
- Nagy, A. F., and T. E. Cravens, Titan's ionosphere: A review, *Planet. Space Sci.*, **46**, 1149, 1998.
- Nagy, A. F., Y. Liu, K. C. Hansen, K. Kabin, T. I. Gombosi, M. R. Combi, and D. L. DeZeeuw, The interaction between the magnetosphere of Saturn and Titan's ionosphere, *J. Geophys. Res.*, **106**, 6151, 2001.
- Phelps, A. V., Cross sections and swarm coefficients for nitrogen ions and neutrals in N₂ and argon ions and neutrals in Ar for energies from 0.1eV to 10 keV, *J. Phys. Chem. Ref. Data*, **20**, 557–573, 1991.
- Schardt, A. W., K. W. Behanon, R. P. Lepping, J. F. Carbary, A. Eviatar, and G. L. Siscoe, The outer magnetosphere, in *Saturn*, edited by T. Gehrels and M. S. Matthews, pp. 416–459, Univ. of Ariz. Press, Tucson, 1984.
- Shematovich, V. I., C. Tully, and R. E. Johnson, Suprathermal nitrogen atoms and molecules in Titan's corona, *Adv. Space Res.*, **27**, 1875, 2001.
- Smith, G. R., D. F. Strobel, A. L. Broadfoot, B. R. Sandel, D. E. Shemansky, and J. B. Holberg, Titan's upper atmosphere: Composition and temperature from the EUV solar occultation results, *J. Geophys. Res.*, **87**, 1351, 1982.
- Stebbins, R. F., B. R. Turner, and A. C. H. Smith, Charge transfer in oxygen, nitrogen and nitric oxide, *J. Chem. Phys.*, **38**, 2277–2279, 1963.
- Stier, P. M., and C. F. Barnett, Charge exchange cross sections of hydrogen ions in gases, *Phys. Rev.*, **103**, 896–907, 1956.
- Yousif, F. B., B. G. Lindsay, and C. J. Latimer, The formation of quasi-bound states of N₂⁺ in H⁺-N₂, *Collisions J. Phys. B At. Mol. Phys.*, **23**, 495–504, 1990.
- Zeigler, J. F., J. P. Biersack, and V. Littmark, *The Stopping and Range of Ions in Solids*, Pergamon, New York, 1985.

R. E. Johnson and M. Michael, Department of Engineering Physics, University of Virginia, Thornton Hall, Charlottesville, VA 22903, USA.

C. J. Latimer, H. Luna, and M. B. Shah, Department of Pure and Applied Physics, Queen's University Belfast, University Road, Belfast BT7 1NN, United Kingdom. (mb.shah@qub.ac.uk)

J. W. McConkey, School of Physical Sciences, University of Windsor, Windsor, Ontario, Canada N9B 3P4.